IOPscience iopscience.iop.org

Home Search Collections Journals About Contact us My IOPscience

Scanning tunnelling spectroscopy of low-dimensional semiconductor systems

This article has been downloaded from IOPscience. Please scroll down to see the full text article.

2004 J. Phys.: Condens. Matter 16 S161

(http://iopscience.iop.org/0953-8984/16/2/019)

View the table of contents for this issue, or go to the journal homepage for more

Download details:
IP Address: 129.252.86.83
The article was downloaded on 28/05/2010 at 07:15

Please note that terms and conditions apply.

INSTITUTE OF PHYSICS PUBLISHING JOURNAL OF PHYSICS: CONDENSED MATTER

J. Phys.: Condens. Matter **16** (2004) S161–S170 PII: S0953-8984(04)66925-6

Scanning tunnelling spectroscopy of low-dimensional semiconductor systems

B Grandidier

Institut d'Electronique et de Microélectronique et de Nanotechnologie, IEMN, (CNRS, UMR 8520), Département ISEN, 41 boulevard Vauban, 59046 Lille Cedex, France

E-mail: grandidier@isen.iemn.univ-lille1.fr

Received 31 July 2003
Published 22 December 2003
Online at stacks.iop.org/JPhysCM/16/S161 (DOI: 10.1088/0953-8984/16/2/019)

Abstract

The applicability of tunnelling spectroscopy by scanning tunnelling microscopy (STM) to semiconductor nanoobjects is addressed through two examples: chemically synthesized PbSe nanocrystals and cleaved InAs quantum dots (QDs) embedded in a GaAs matrix. In the case of free-standing nanocrystals on a metallic substrate, measurements of the conductance at low temperature provides the electronic structures of the nanocrystals in the conduction band and a broad transition range is found for the density of states as a function of the nanocrystal dimensions. Use of the scanning ability of the STM also allows the acquisition of spectroscopic images. At room temperature, current images obtained on cleaved InAs QDs for different samples voltages show the formation of standing wave patterns, which are identified as the probability density of the ground and first excited states. Such results open the opportunity to study the electronic structure of more complicated systems based on the assembly of semiconductor nanoobjects such as coupled QDs.

1. Introduction

Different methods of growth or synthesis of low-dimensional semiconductors allow the fabrication of small objects where the dimensions can widely vary, leading thus to quantum size effects. As the sizes of the semiconductor structures are in the nanometre range, specific tools are required to observe these nanoobjects and characterize simultaneously the quantum size effects. Scanning tunnelling microscopy (STM) offers the possibility to image the surfaces of individual nanostructures and, when used in the spectroscopic mode, can probe the electronic structure of single objects. While this technique has been extensively used to study metallic objects [1] or surface states of semiconductor surfaces [2], it has been proven more recently to be well suited to determining the electronic structure of semiconductor nanoobjects, if their surface states lie far from the band edges [3, 4].

In this paper, we report the results of spectroscopic measurements obtained on two types of semiconductor nanoobjects and discuss the limits of this technique. Although variations of their size modify significantly their electronic structure, other effects must generally be taken into account to interpret the tunnelling spectra, such as the electron–electron Coulomb interaction. However, in this paper, the electron–electron Coulomb interaction is turned off, either by working with a small tunnelling barrier between the nanoobjects and the substrate on which they are lying, or by choosing a very low current setpoint, which corresponds to a thick tunnelling barrier between the tip and the nanoobject. Thus, the experiments are all conducted in a regime, called the shell-tunnelling regime, where the electron levels of the nanoobject are occupied by a single electron.

As a first example of tunnelling spectroscopic measurements on semiconductor nanostructures, we investigate the variation of the density of states (DOS) as a function of the size of lead selenide (PbSe) particles, deposited onto a metallic surface. The shape-controlled fabrication of these particles allows the formation of flat nanocrystals with different lateral size to height aspect ratio. Substantial changes of the DOS are expected when the lateral size decreases and approaches the height of the nanocrystal. Low-temperature tunnelling spectroscopy, supported by electronic structure calculations, reveals a wide transition region, in which the DOS function shows a rich and varied structure, featuring steps and peaks.

Although the electron energy levels are well resolved for such particles by tunnelling spectroscopy at low temperatures, the acquisition of single curves is generally noisy, probably due to the synthesis of the particles in a solution and their exposure to the air prior to their loading into an ultra-high vacuum (UHV) environment. Therefore, the current and the conductivity measurements are strongly averaged. As the observation of the probability density requires the formation of a spatial conductivity map from the acquisition of a single measurement at each point of the STM image, the time to obtain such a result may become quite long and make these experiments difficult to achieve. On the other hand, semiconductor nanoobjects embedded in a semiconductor host can be exposed to the tip of the STM after the cleavage of the crystal in UHV. In this case, the measurements are quite stable, and even at room temperature the spatial variations of single current–voltage characteristics are meaningful. As an example, we show results obtained on cleaved InAs quantum dots (QDs) embedded in GaAs, where the probability density variations are clearly resolved for the first electron levels in the conduction band. Such a method to observe the electron amplitude wavefunction is then applied to doubly stacked InAs QDs in GaAs in order to determine the electronic coupling between the dots.

2. Density of states of PbSe nanocrystals

The growth of PbSe nanocrystals by electrodeposition onto a gold substrate is anisotropic and favours the formation of two-dimensional films. By controlling the total charge during the electrodeposition process, flat nanocrystals can be obtained, and depending on the lateral sizes of the nanocrystals, significant variations of the electronic structures are expected between the widest nanocrystals and the smallest nanocrystals. Using an aqueous solution of $Pb(CH_3COO)_2$ and H_2SeO_3 [5], PbSe nanocrystals were electrodeposited onto flame annealed Au(111) surfaces by interrupted bulk deposition at -0.5 V versus SCE. While the formation of lead selenide nanocrystals was confirmed by x-ray diffraction analysis and high resolution transmission electron microscopy, STM images and linecuts through the nanocrystals obtained from the images, such as the one shown in figure 1, indicate that the height of the nanocrystals is smaller than the width. When the amount of charge used for deposition is less than 3.0 mC cm^{-2}, the height of the nanocrystals varies between 4 and 8 atomic layers of PbSe, whereas a wide range of lateral sizes—from a few to more than 20 nm—is found. As the

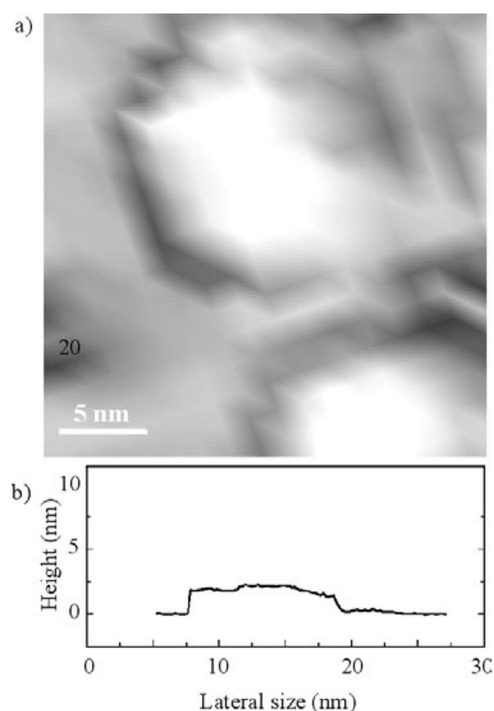

Figure 1. STM topographic image of flat PbSe nanocrystals. The colour scale ranges from 0 (dark) to 3 nm (bright).

top surface exhibits height variations smaller than the lattice constant of PbSe (0.61 nm), the nanocrystals are flat and they show a brick-like shape, complying with the rocksalt structure of lead-salt crystals [4].

By positioning the tip at the centre of a brick-shaped nanocrystal, separated from its neighbours by 2 nm at least, spectroscopic measurements of individual nanocrystal can be performed. Both the tunnelling current I and the differential conductivity $\mathrm{d}I/\mathrm{d}V$ are recorded while the voltage between the tip and the sample is scanned. The differential conductivity was generally acquired by applying a modulation amplitude of 6 mV rms at a frequency of 1 kHz. In the case of the smallest nanocrystals, the spectroscopic measurements were made at constant tip-to-sample separations, otherwise the nanocrystals could easily be moved during the measurements. On the wider nanocrystals, spectroscopic measurements were obtained first at fixed tip-to-sample distance to determine the zero of the current and the conductivity and then with an additional tip-to-sample approach in the zero-conductivity gap in order to induce a variation of the electron-barrier transmission factor and probe small densities of states within the band gap [6]. As a result, in order to characterize the DOS of individual nanocrystals, we use the normalized conductivity $(\mathrm{d}I/\mathrm{d}V)/(I/V)$, since this quantity was shown to be independent of the transmission factor [7]. So that it does not diverge for voltages close to zero, $(\mathrm{d}I/\mathrm{d}V)/(I/V)$ was furthermore calculated by adding a small constant to the absolute value of the tunnelling current [8].

Figure 2 shows three $(\mathrm{d}I/\mathrm{d}V)/(I/V)$ spectra obtained on brick-shaped nanocrystals with the same height (1.5 nm) and edges ranging from 21 to 2.7 nm, respectively. The fourth spectrum was measured on a cubic nanocrystal with edges of 2.4 nm. Each spectrum is obtained by averaging over many successive measurements for the same tip position (up to

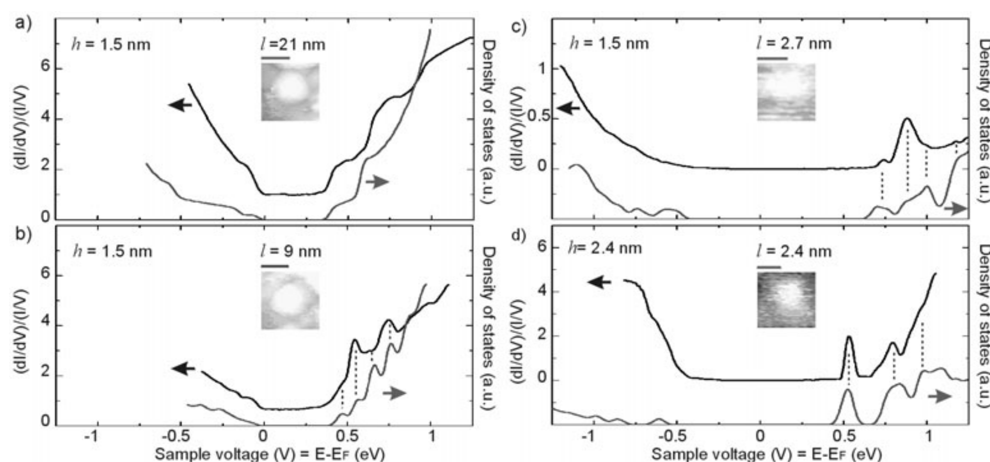

Figure 2. Experimental normalized conductivity and theoretical DOS of PbSe nanocrystals. The three first nanocrystals (a), (b), (c) all have a height of 5 atomic layers. The fourth spectrum (d) has been obtained on a nanocrystal with a height of 8 atomic layers. For each nanocrystal, the length of the scale bar corresponds to the L-value used to calculate the DOS. As $(dI/dV)/(I/V)$ is zero in the band gap for the smallest nanocrystals, the DOS has been shifted for the two final spectra. The vertical dotted lines indicate the position of the peaks for comparison.

150 for spectrum 2). The figures exhibit the conduction states at positive voltages and the valence states at negative voltages. The spectrum of a nanocrystal with an aspect ratio of 14 (figure 2(a)) is dominated by steps in the conduction and valence bands and shows a band gap of 0.45 eV, i.e., much larger than that of bulk PbSe (0.15 eV at 4.2 K). The steps correspond to the onset energies of the electron and hole subbands. Their appearance and the widening of the band gap is a clear signature of the DOS of a 2D semiconductor. If the aspect ratio is reduced to 6, the band gap (0.50 eV) increases slightly and a peak structure is observed in the conduction band (figure 2(b)). The appearance of a more complex DOS structure is attributed to the reduction of the edge length. Further reduction of the aspect ratio to 2 leads to a strong increase of the band gap (approximately 1.10 eV) and a more pronounced peak structure in the conduction band (figure 2(c)).

For the cubic nanocrystal with dimensions of 2.4 nm, two peaks in the conduction band are observed (figure 2(d)). Between the peaks, the DOS approaches zero and the confinement in this nanocrystal has the property of an 0D system. Comparison of the spectrum obtained for this nanocrystal and that with $h = 1.5$ nm and $L = 2.7$ nm demonstrates that the DOS depends critically not only on the strength of the confinement but also on the shape of the nanocrystal. Although the nanocrystal with $h = 1.5$ nm contains fewer atoms than the nanocrystal with $h = 2.4$ nm, it has a lower symmetry, which prevents it from having the property of a true 0D electronic system.

In the spectra of the largest nanocrystals, the band gap is not positioned symmetrically around zero volt, which corresponds to the Fermi level position. Such a Fermi level shift towards the valence band can indicate a transfer of charge from the Au(111) surface to the nanocrystals, comparable to what was observed for a carbon nanotube on the Au(111) surface [9]. As a result, $(dI/dV)/(I/V)$ exhibits a non-zero value of 1 and 0.65 in the band gap region for the nanocrystals with aspect ratio 14 and 6, respectively. Upon reduction of the aspect ratio, the band gap widens and the electrostatic screening is reduced. As a consequence, $(dI/dV)/(I/V)$ reaches zero and the Fermi level shifts to a more symmetric position.

A tight-binding calculation of the electronic structure of isolated brick-shaped PbSe nanocrystals, using a $sp^3d^5s^*$ basis and taking into account a screening surface potential [10], agrees with the band gap values and the peak positions in the conduction band for the different nanocrystals, as shown by the grey coloured curves in figure 2. However, discrepancies between experiment and theory exist and may account for the conduction band variation with small deviations from the brick shape, which are beyond the resolution of the STM, or to SeO_3^{2-} groups terminating the PbSe surface. Regarding the variations of the valence band, steps can be observed in the different spectra, but no peaks appear when the aspect ratio is decreased. The non-appearance of peaks may be caused by a strong decrease of the tunnelling transmission at lower energy, as already observed in the case of other semiconductors [11, 12].

3. Probing the quantum states of InAs dots

The controlled growth of InAs on a GaAs substrate in the Stransky–Krastanow growth mode leads to the fabrication of pseudomorphic QDs. These dots exhibit a three-dimensional confinement with a δ-function-like electronic DOS. As the electron ground and first excited states in these dots are generally separated by a few tens of millielectronvolts, the energy of both states can be resolved by tunnelling spectroscopic techniques at room temperature. In recent years, scanning tunnelling spectroscopy (STS) has provided a unique means to obtain not only the electronic spectra of low-dimensional structures but also the localization of the spectral features. The observation of the charge densities was for example achieved in artificial structures like the quantum corral [13] or even at room temperature on natural scattering centres like surface steps [14]. As a result, the probability density of electrons in InAs QDs can be investigated by STS.

The InAs QDs were grown by molecular beam epitaxy on an (001)-oriented GaAs substrate, with a residual p-type concentration. The active part of the samples consists of 15 arrays of InAs boxes separated by 15 nm GaAs barriers. The whole structure is covered by a 140 nm GaAs overlayer. In order to build each dot array, 2.3 monolayers of InAs were deposited on the GaAs layer within 20 s at a temperature of 520 °C. They were immediately buried with GaAs. With these growth conditions, the density of dots is as high as 10^{10} cm^{-2} in the (001) plane. As cubic zinc-blende-structure compound semiconductors cleave easily along their nonpolar (110) planes, a large number of InAs QD cross-sections are observed with the STM. When the cleavage is achieved in UHV after thinning back the rear side of the sample, defect-free surfaces are usually obtained and since these surfaces are electronically unpinned, tunnelling spectroscopy allows the determination of the bulk electronic properties, such as the band gap or the electron subbands of quantum wells [11].

In figure 3, we display a cross-sectional topographic STM image of a stack of self-aligned QD along the [001] growth direction. The QD appear bright and the GaAs layers dark. The four dots are lying on bright layers which correspond to the wetting layers. We may expect the dots, that show the largest sizes and the highest contrast, to be cleaved near the dot centre, leaving one half of the dots underneath the cleavage plane. We will now focus on such dots, where the confined electron states can easily be resolved. In general, these dots have a length around 20 nm and their height ranges from 4 to 5.6 nm.

The STM contrast depends on both the topographic variations of the surface and the electronic structure of the underlying layer. As the InAs QDs are compressively strained in GaAs, the (110) cross-section of a QD is displaced outward due to the relaxation of the materials after the cleavage. Such displacement causes a bright contrast in the STM images in agreement with the observed contrast in figure 3. However, the DOS in the QDs is higher than the one in the GaAs layer when energies below or at the bottom of the GaAs conduction band

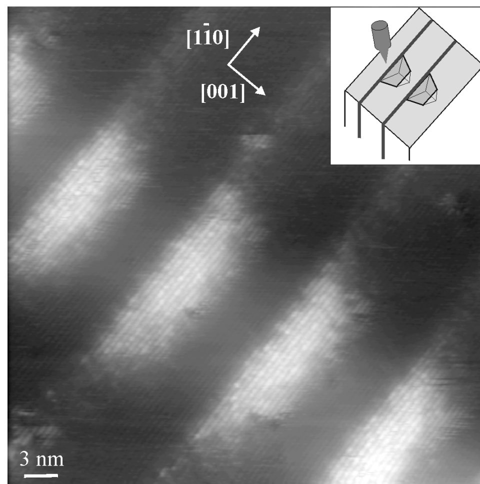

Figure 3. STM image of the (110) face of an InAs dot-stack layer in GaAs. The image was acquired at a sample bias of 1.86 V. Inset: schematic diagram of the cleave.

edge are probed. At low sample voltages, their contribution is thus significant in the tunnelling current, and to keep the tunnelling current constant, the tip is retracted when it scans a QD, which also induces a bright contrast in the STM image. As the sensitivity of the spectroscopic measurements depends strongly on the tip–sample separation, we need first to estimate the relative contributions of both effects, so that $I(V)$ spectra can be compared no matter where they are acquired, either in the middle of a QD, in the edges or in the GaAs layers.

The mechanical effect can be determined by calculating the strain relaxation of cleaved InAs dots embedded in GaAs. A truncated pyramid like an InAs dot, with a 20 nm [100] $\times$ [010] square base and {110} faces, was considered in the calculation. The truncated pyramid lies on a 0.4 nm thick wetting layer. The calculated box was cleaved perpendicular to the [110] direction, along the main diagonal of the square base. Strain relaxation at the cleaved edge was calculated with a finite difference method within continuum elasticity theory, following the work of Grundmann *et al* [15].

Figure 4(a) shows the calculated structural height variation at the cleavage surface due to the strain relaxation. For comparison, a contour line plot obtained from the central dot on the STM image in figure 3 is plotted in figure 4(b). Both the computation and the experimental observation give a height variation of 4 Å. At voltages higher than +1.86 V, the strain relaxation is thus the major source for the contrast between the box and the surrounding layer. Therefore the tip-to-sample distance can be considered as being the same when the tip is located either above a dot, a wetting layer or the GaAs spacers.

To investigate the electronic structure of a dot, tunnelling current voltage curves were acquired simultaneously with the topographic image above individual quantum dots. At every point of the image, obtained with a sample voltage of +2.15 V, the feedback loop was switched off to measure the I–V curves. During an $I(V)$ measurement, the vertical position of the tip is held stationary. A current image at a given voltage is then drawn by plotting at each point of the image the value of the current obtained at this point during the I–V measurement. The results are displayed in figure 5. Figure 5(a) is the topographic image of a QD. This particular dot has a base length of 20 nm and a height of 4 nm. The current images are displayed in figures 5(b) and (c). They were obtained for an applied voltage of +0.69 and +0.82 V, respectively. In these images, regions of high current are bright and regions of low current

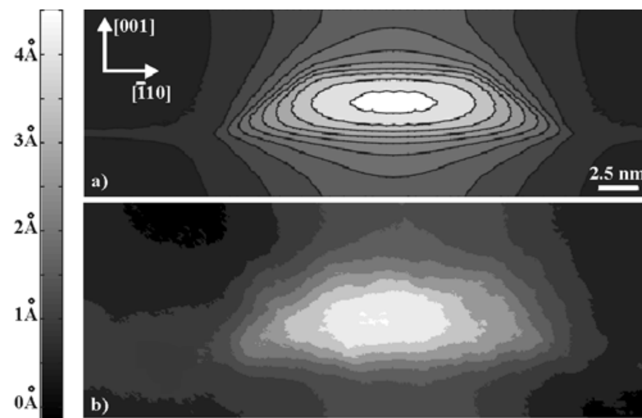

Figure 4. Comparison of the height variation between (a) a simulated topographical image and (b) an STM image of the cleaved InAs dot located in the centre of figure 3. A low pass filter was used to remove the atomic corrugation from figure 4(b). For clarity, a contour line plot is displayed.

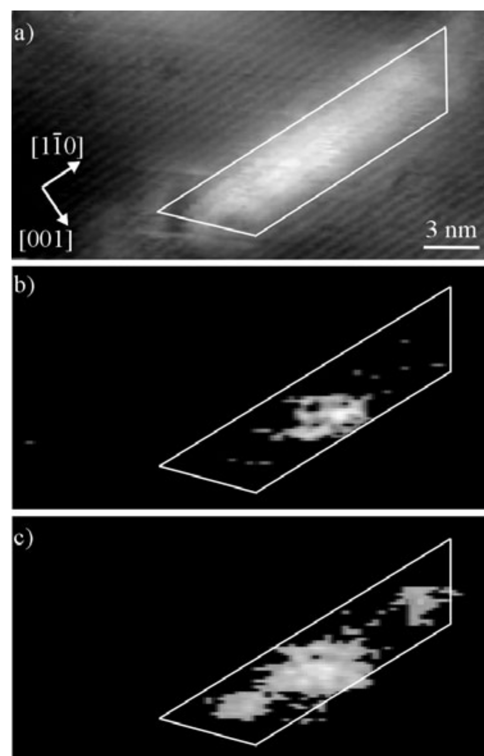

Figure 5. Simultaneously acquired topographic and current images of an InAs QD: (a) STM topograph with +2.15 V, applied to the sample, current images at a sample bias of (b) +0.69 V and (c) +0.82 V. The boundaries of the dot, determined from figure (a), are outlined in each image. The grey scale ranges from 0.01 to 0.8 and 1.5 pA for figures (b) and (c), respectively.

are dark. While figure 5(a) outlines the dot contour, the current image in figure 5(b) shows a standing wave pattern in the centre of the dot. The intensity of this feature varies with voltage:

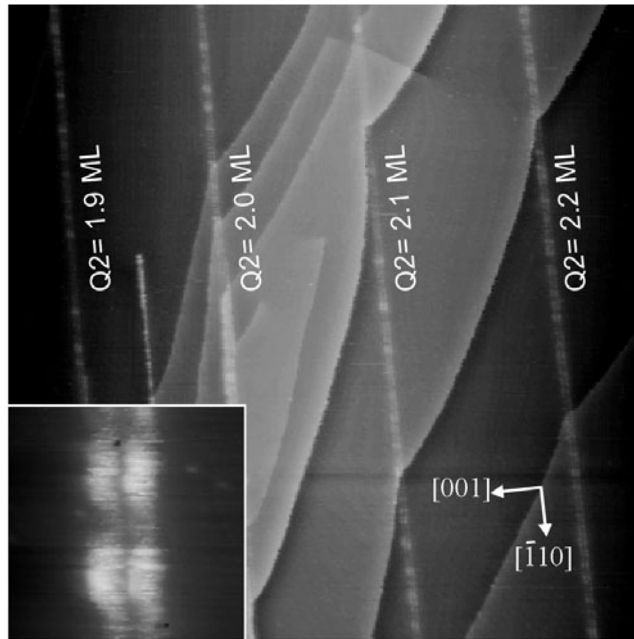

Figure 6. Cross-sectional STM images of doubly stacked InAs QD arrays in GaAs. The growth direction is from the right to the left. The coverage of the second array Q2 is given for each bilayer. Numerous step edges are seen in the image due to the difficulty in cleaving samples containing a large quantity of bilayers. Image size: 600 nm × 600 nm. Inset: Two doubly stacked InAs QDs observed in the bilayer with a coverage of 1.9 monolayers. Image size: 30 nm × 30 nm.

it becomes clearly visible at a voltage of +0.63 V and its intensity increases up to +0.74 V. At a voltage of +0.74 V, the standing wave pattern suddenly changes. Two new features are now apparent surrounding the central feature in the [1$\bar{1}$0] direction, as shown in figure 5(c). Their intensity increases with voltage up to +0.9 V. For sample voltages larger than +0.9 V, the dot becomes brighter and brighter with no other distinct feature visible in the dot. For such large voltages, we may expect to tunnel into the empty states of the wetting layer and the GaAs conduction band [16].

As it was previously shown that the tip–sample separation is insensitive to the electronic effects for a voltage of +2.15 V, the wave patterns in figures 5(b) and (c) are obtained without the interference of mechanical contributions and so reflect the spatial distribution of the lowest electron states confined in the dot. As only the states lying between the Fermi levels of the sample and of the tip contribute to the tunnelling process, the standing wave pattern at a voltage of +0.69 V corresponds therefore to the probability density of the electron ground state in the dot, whereas at a voltage of +0.82 V, the standing wave pattern can be regarded as a combination of the probability densities of the electron ground and first excited states. The ground state has a s-like shape and the first excited state a p-like shape with one nodal plane. Similar results have been obtained more recently with InGaAs and uncapped InAs QDs grown on GaAs. In the case of InGaAs dots, the authors report on the observation of the spatial variation of the confined hole wavefunction at room temperature [17]. As for the uncapped InAs QDs, the spectroscopic measurements were performed at low temperatures and due to the small drift of the scanner, not only current but also conductivity images can be recorded and the probability densities of up to four electron states were observed [18].

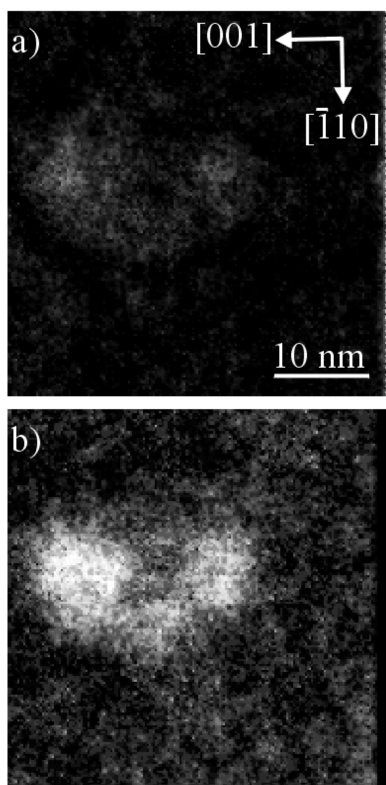

Figure 7. Current images of a stack of 2 dots separated by 1.8 nm. Images (a) and (b) were obtained for a sample bias of +0.28 and +0.32 V, respectively. The grey scale ranges from 0.01 to 0.4 and 2.0 pA for figures (a) and (b), respectively.

4. Future prospect

While the probability densities of confined carriers have been resolved for single dots, the spatial mapping of quantum states by STS can also be applied to more complicated structures, like closed stacked bilayers of QDs. As shown in figure 3, the growth of successive arrays of InAs QDs separated by thin GaAs spacers leads to a vertical alignment of the QDs along the growth direction [19]. If the spacer thickness is reduced to a few nanometres, electronic coupling between the dots can be expected, since the shape and the composition of the dots of two successive arrays are almost similar. A strong electronic coupling corresponds to the delocalization of the electron wavefunction and such delocalization should be detectable in the current images.

Bilayers of InAs QD arrays, separated by a 3 nm GaAs spacer, have been grown by molecular beam epitaxy. The first array was built by depositing 2.3 monolayers of InAs on a GaAs layer. To adjust the dot size of the second array to the dot size of the first array, the InAs coverage was varied between 1.2 and 2.3 monolayers. Figure 6 shows a cross-section STM image of different bilayers for coverages ranging from 2.3 to 1.9 monolayers for the second array. The bilayers appear as bright double lines extending perpendicular to the [001] growth direction. The brightest protrusions in the bilayer correspond to doubly stacked dots. As shown in the inset of figure 6, dots of similar sizes in both arrays are generally found

when the coverage of the second layer is 1.9 monolayers. This result was also confirmed by cross-sections of the sample obtained by transmission electron microscopy. In between the dots, the Ga(In)As tunnel barrier has a thickness of 1.8 nm. Such a small thickness should in principle make the electronic coupling between the dots possible.

To attest an electronic coupling, we adopt the same procedure as the one used to probe the probability density of single dots: maps of $I(V)$ curves were acquired in the bilayer where the coverage of the second layer corresponds to 1.9 monolayers. Two current images of a stack of two QDs are shown in figure 7 for two different positive sample voltages. For such small voltages, the ground state is probed and we can observe that the ground state of the upper dot (Q2) appears brighter than the one of the lower dot (Q1). Both states are mainly localized in the dots and it is clear that the QDs are not coupled. We have examined seven stacks of double dots and similar results were found: the wavefunctions of the ground states are not delocalized. While most of the QDs in both layers seem to have the same height, cross-sectional STM images do not show the entire volume of the dots and the vertical size of the QD may vary slightly below the cleavage plane. As the dot band gap is very sensitive to such small fluctuations, these variations of the geometry may explain the non-coupling of the dots.

Acknowledgments

The author is grateful to G Allan, C Delerue, D Deresmes, J M Gérard, Z Hens, B Legrand, Y M Niquet, J P Nys, C Priester, D Stiévenard, V Thierry-Mieg, and D Vanmaekelbergh, who contributed in various ways to this work.

References

[1] Li J, Schneider W-D, Berndt R and Crampin S 1998 *Phys. Rev. Lett.* **80** 3332
[2] Becker R S, Golovchenko J A, Hamann D R and Swartzenruber B S 1985 *Phys. Rev. Lett.* **55** 2032
[3] Banin U, Cao Y, Katz D and Millo O 1999 *Nature* **400** 542
[4] Hens Z *et al* 2002 *Phys. Rev. Lett.* **88** 236803
[5] Molin A N and Dikusar A I 1995 *Thin Solid Films* **265** 3
[6] Mårtensson P and Feenstra R M 1988 *Phys. Rev.* B **39** 7744
[7] Feenstra R M, Stroscio J A and Fein A P 1987 *Surf. Sci.* **181** 295
[8] Prietsch M, Samsavar A and Ludeke R 1991 *Phys. Rev.* B **43** 11850
[9] Wildoer J W G *et al* 1998 *Nature* **391** 59
[10] Niquet Y M, Delerue C, Allan G and Lannoo M 2000 *Phys. Rev.* B **62** 5109
[11] Feenstra R M, Collins D A, Ting D Z Y, Wang M W and McGill T C 1994 *Phys. Rev. Lett.* **72** 2749
[12] Feenstra R M 1994 *Phys. Rev.* B **50** 4561
[13] Crommie M F, Lutz C P and Eigler D M 1993 *Nature* **363** 524
[14] Avouris P and Lyo I W 1994 *Science* **264** 942
[15] Grundmann M, Stier O and Bimberg D 1995 *Phys. Rev.* B **52** 11969
[16] Grandidier B, Niquet Y M, Legrand B, Nys J P, Priester C, Stiévenard D, Gérard J M and Thierry-Mieg V 2000 *Phys. Rev. Lett.* **85** 1068
[17] Johal T K, Rinaldi R, Passaseo A, Cingolani R, Vasanelli A, Ferreira R and Bastard G 2002 *Phys. Rev.* B **66** 75336
[18] Wiesendanger R 2003 private communications
[19] Legrand B, Nys J P, Grandidier B, Stiévenard D, Lemaitre A, Gérard J M and Thierry-Mieg V 1999 *Appl. Phys. Lett.* **74** 2608